CMS Physics Analysis Summary

Contact: cms-pag-conveners-exotica@cern.ch 2014/06/10

Search for Contact Interactions in Dilepton Mass Spectra in pp Collisions at $\sqrt{s} = 8\,\text{TeV}$

The CMS Collaboration

Abstract

A search for contact interactions in events with muon or electron pairs has been performed. The data samples were collected by the CMS detector and correspond to integrated luminosities of 20.6 and 19.7 fb^{-1} for the muon and electron channels, respectively, for proton-proton collisions at $\sqrt{s} = 8\,\text{TeV}$. Within the context of a quark and lepton compositeness model with a left-left isoscalar contact interaction, 95% CL lower limits are set on Λ, the energy scale parameter for the contact interaction. For dimuons the limits are 12.0 and 15.2 TeV for destructive and constructive interference with Drell–Yan production, respectively; for dielectrons the limits are 13.5 and 18.3 TeV. These limits are the most stringent to date.

1 Introduction

This note describes a search for contact interactions (CI) in the dimuon and dielectron channels using pp collision data at $\sqrt{s} = 8\,\text{TeV}$ collected by the Compact Muon Solenoid (CMS) detector at the Large Hadron Collider (LHC). The muon channel corresponds to an integrated luminosity of $20.6\,\text{fb}^{-1}$ while the electron channel corresponds to $19.7\,\text{fb}^{-1}$.

The existence of three families of quarks and leptons might be explained if these particles are composed of more fundamental constituents. In order to confine the constituents and to account for the properties of quarks and leptons, a new strong gauge interaction, metacolor, is introduced. Below a given interaction energy scale Λ, the effect of the metacolor interaction is to bind the constituents into metacolor-singlet states. For parton-parton center-of-mass energies less than Λ, the metacolor force will manifest itself in the form of a flavor-diagonal CI [1]. We consider the left-left isoscalar model (LLIM) [2], which is the conventional benchmark for CI in the dilepton channel. In the LLIM the Lagrangian density is given by

$$\mathcal{L} = \frac{g^2}{2\Lambda^2}(\eta_{LL}\bar{q}_L\gamma^\mu q_L\bar{l}_L\gamma_\mu l_L), \tag{1}$$

where $q_L = (u,d)_L$ is a left-handed quark doublet, l_L is a left-handed lepton, and g and η_{LL} are constants. By convention $g^2/4\pi = 1$. For maximum destructive interference $\eta_{LL} = +1$ and for maximum constructive interference $\eta_{LL} = -1$. In this analysis, all flavors of initial-state quarks are assumed to be composite.

The dileptons from the subprocesses for standard model (SM) Drell–Yan (DY) [3] production and from CI production can have the same helicity state. In this case, the scattering amplitudes are summed, resulting in an interference term in the cross section for $pp \to l^+l^- + X$. The differential cross section corresponding to the combination of CI production described by Eq. (1) with DY production can be written as

$$\frac{d\sigma^{\text{CI/DY}}}{dM} = \frac{d\sigma^{\text{DY}}}{dM} - \frac{\eta_{LL}}{\Lambda^2}\mathcal{I}(M) + \frac{\eta_{LL}^2}{\Lambda^4}\mathcal{C}(M), \tag{2}$$

where M is the invariant dilepton mass, $\mathcal{I}$ is due to interference, and $\mathcal{C}$ is purely due to the CI. The processes contributing to the cross section in Eq. (2) are denoted collectively by "CI/DY". The signal for a contact interaction is the difference

$$\frac{d\sigma^{\text{CI/DY}}}{dM} - \frac{d\sigma^{\text{DY}}}{dM}. \tag{3}$$

The basic features of the LLIM dilepton mass spectra are demonstrated with a generator-level simulation using PYTHIA v6.4 [4], with appropriate kinematic selection criteria that approximate the acceptance of the detector. Figures 1a and 1b show the LLIM dimuon mass spectra for different values of Λ for destructive and constructive interference, respectively. The curves illustrate that with increasing mass the CI leads to a less steeply falling yield relative to DY production, with the effect most prominent at low values of Λ and steadily diminishing with increasing values of Λ. For a given value of Λ and dilepton mass, the event yield is seen to be larger for constructive interference compared with the destructive case. As Λ increases the CI/DY yield approaches the DY yield, as expected from Eq. 2.

Previous searches for contact interactions in dijet and dilepton channels have all resulted in limits on Λ. Searches have been reported by experiments at LEP [5–9], HERA [10, 11], the Tevatron [12–17], and recently from the ATLAS [18–21] and CMS [22–26] experiments at the

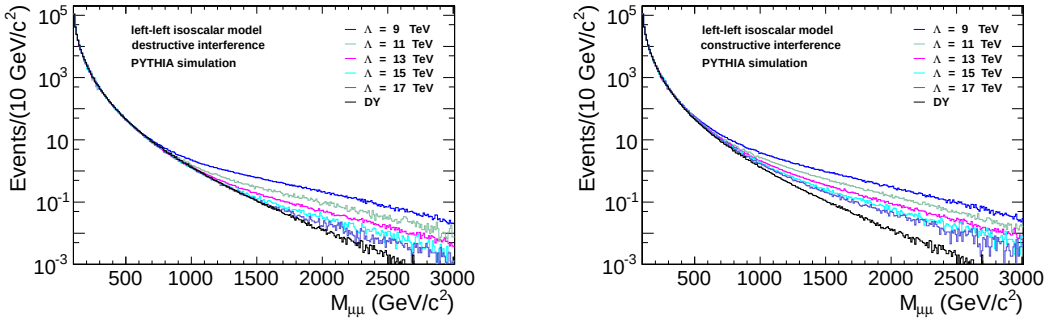

(a) (b)

Figure 1: Simulated dimuon mass spectra using the left-left isoscalar model for different values of Λ for (a) destructive interference and (b) constructive interference. The events are generated using the PYTHIA Monte Carlo program with kinematic selection requirements that approximate the acceptance of the detector and the yields correspond to an integrated luminosity of 20 fb^{-1}. The corresponding curves for dielectrons are similar.

LHC. The highest published limits in the LLIM dimuon channel for a hadron collider are from ATLAS and CMS 7 TeV data. For destructive interference, these limits are 9.5 TeV (CMS) and 9.6 TeV (ATLAS). For constructive interference the limits are 13.1 TeV (CMS) and 12.9 TeV (ATLAS). ATLAS also reported limits in the dielectron channel based on 7 TeV data, and these are 9.5 TeV and 12.1 TeV for destructive and constructive interference. There are larger limits [27] in the eeuu channel, $\Lambda > 23.3$ TeV ($\Lambda > 12.5$ TeV) for destructive (constructive) interference, and in the eedd channel, $\Lambda > 11.1$ TeV ($\Lambda > 26.4$ TeV), although these are based on combination of results from a number of sources.

2 CMS Detector

CMS uses a right-handed coordinate system with origin at the nominal collision point, the x axis pointing toward the center of the LHC ring, the y axis perpendicular to the LHC plane and pointing vertically upward, and the z axis along the anticlockwise beam direction. Pseudorapidity η is defined as $\eta = -\ln[\tan(\theta/2)]$ where θ is the polar angle relative to the z axis. The azimuthal angle ϕ is measured relative to the positive x axis in the x-y plane.

The main CMS systems used in this analysis include the tracker and calorimeters, both of which are located inside the 3.8 T superconducting solenoid, and the muon system, which has detection elements interspersed in the return yoke of the solenoid. The tracker consists of silicon pixel and strip systems and measures charged particle trajectories within the pseudorapidity range $|\eta| < 2.5$. The electromagnetic calorimeter (ECAL) consists of nearly 76 000 lead-tungstate crystals and provides coverage up to $|\eta| = 3.0$. The brass and scintillator hadronic calorimeter surrounds the ECAL and aids it in identifying electrons. The muon detectors include drift tubes, resistive plate chambers, and cathode strip chambers. Muons are reconstructed in the range $|\eta| < 2.4$ although the coverage of the single muon trigger extends only up to $|\eta| = 2.1$. The tracker, calorimeters, and muon systems all have barrel and endcap components. A detailed description of the CMS detector can be found in Ref. [28].

The first level (L1) trigger selects events based on a sub-set of information from the muon detector and the calorimeters. The High Level Trigger (HLT) processor farm then filters L1

triggers using full information from the tracker, calorimeters, and muon system. Events that have been selected by the HLT are then written to either the single muon or diphoton data streams, depending on the trigger path.

3 Trigger and event reconstruction

The trigger and reconstruction method used here is the same as used in searches for a narrow dilepton resonance [29] and extra spatial dimensions in dimuon [30] and dielectron [31] production. This allows for common dilepton spectra to be interpreted in the context of different new physics models.

3.1 Dimuon channel

Dimuon events are recorded with a trigger requiring a single muon with $p_T > 40\,\text{GeV}$. For single muon triggers, triggering muons are restricted to the range $|\eta| < 2.1$ in order to avoid a high rate of low-p_T muons that would be mis-reconstructed as exceeding the p_T threshold due to their poorer p_T resolution. The integrated luminosity for this trigger is $20.6\,\text{fb}^{-1}$. At least one muon of the dimuon pair must be matched to the trigger muon, meaning $\Delta R = \sqrt{(\Delta\eta)^2 + (\Delta\phi)^2} < 0.2$ and $\Delta p_\text{T}/p_\text{T} < 1$; the other muon is limited to $|\eta| < 2.4$ by the geometrical acceptance of the muon system. For dimuon masses above 200 GeV the trigger efficiency is $\sim 97\%$.

Muons must be reconstructed in both the tracker and the muon detector. Each muon track is required to have a signal ("hit") in at least one pixel layer, hits in at least six strip layers, and multi-hit segments in at least two muon detector stations. Both muons are required to have $p_\text{T} > 45\,\text{GeV}$ and a p_T reconstruction accuracy $\delta p_\text{T}/p_\text{T} < 0.3$. To reduce the cosmic ray background, the transverse impact parameter of the muon with respect to the primary vertex is required to be less than 0.2 cm. The primary vertex is taken to be the pp collision within the bunch crossing with the highest summed p_T^2 over all charged tracks associated with the vertex. In order to suppress muons coming from hadronic decays, a tracker-based isolation requirement is imposed such that the p_T sum of all tracks with z-values (in the interaction region) within 0.2 cm of the z-value of the muon and within $\Delta R = 0.3$ with respect to the muon track is less than 10% of the p_T of the muon.

The two muons are required to have opposite charge and must be consistent with originating from a common vertex. A constrained fit of the muon tracks to a common vertex must satisfy $\chi^2/\text{dof} < 10$. To further suppress cosmic ray muons that are in time with the collision event, the 3-dimensional angle between the two muons must be smaller than $\pi - 0.02$ radians.

3.2 Dielectron channel

Dielectron events are recorded with a trigger requiring two electrons, each with $E_\text{T} > 33\,\text{GeV}$ and the integrated luminosity for this trigger is $19.7\,\text{fb}^{-1}$. Electrons candidates start as superclusters in the ECAL, although only one supercluster is required for the L1 trigger. Both superclusters must have no more than one missing hit in the pixel layers and the fraction of HCAL energy associated with each cluster must be less that 15% of the ECAL energy. For dielectron masses above 200 GeV the trigger efficiency is $\sim 99\%$.

Offline, individual electrons must have $E_\text{T} > 35\,\text{GeV}$. The pseudorapidity coverage is $|\eta| < 1.442$ in the barrel and $1.56 < |\eta| < 2.5$ in the endcaps. For each electron, the ECAL cluster must match the tracker trajectory within 0.005 (0.007) in η and 0.06 (0.06) in ϕ for barrel (endcap) candidates. The ratio of hadronic to electromagnetic energy deposition must be less than

0.05 for both barrel and endcap candidates. To increase the likelihood that the electrons were produced at the primary vertex, the electron track's transverse impact parameter with respect to the primary vertex is required to be less than 0.02 (0.05) cm for barrel (endcap) candidates. To suppress hadrons from jets that could be mis-identified as electrons, an isolation requirement is imposed based on a cone with $0.04 < \Delta R < 0.30$ centered on the electron track. Within this cone the p_T sum of all tracks (with $p_T > 0.7$ GeV and z-values within 0.2 cm of the electron z-value in the interaction region) is required to be less than 5 GeV. Similarly, the summed E_T in the same cone is required to be less than 3% of the E_T of the electron candidate, where a correction is applied to the summed E_T to account for pileup effects in the ECAL [32].

At least one of the electrons in a dielectron pair must be reconstructed in the barrel and both electrons must match trigger objects. However, for dielectrons there is no requirement that the electrons be oppositely charged. This helps recover some dielectron pairs where one of the charges has been mis-identified. Since the electron E_T measurement comes from the ECAL, this is unaffected by a mismeasurement of charge within the tracker.

4 Signal and background prediction

In this section we describe the prediction for the observed number of events from CI/DY production, pure DY production, and non-DY SM backgrounds. The predictions are made with physics generators followed by a full detector simulation using GEANT4 [33]. For the dielectron channel, the background from QCD jets is estimated using a combination of simulation and a mis-identification rate determined from data [29].

4.1 Drell–Yan NLO samples

Simulations samples based on the next-to-leading order (NLO) event generator POWHEG [34] with the CT10 PDF [35] are used to determine the DY backgrounds, both for comparison with data and for establishing lower limits on Λ as described in Section 7. The samples were generated with minimum $\sqrt{\hat{s}}$ values of 120, 200, 500, 800, 1000, 1500, and 2000 GeV for dimuons and 120, 200, 400, 500, 700, 800, 1000, 1500, and 2000 GeV for dielectrons. Each sample contains approximately 100k events. An additional multiplicative factor of 1.024 is applied as a QCD NNLO correction [29] to the POWHEG yields, and a 3% uncertainty is assigned to this based on observed variations in the NNLO correction as a function of dimuon mass. The POWHEG samples are also used to determine the systematic uncertainties in the event yield predictions due to variations within PDF sets and between sets.

4.2 Contact Interaction samples

Using the LLIM, CI/DY events are generated using the leading-order (LO) generator PYTHIA v6.4 [4] with the CTEQ6L1 parton distribution functions [36]. CI/DY samples were generated for both dimuons and dielectrons for Λ values of 9, 11, 13, and 15 TeV for destructive interference, Λ values of 9, 11, 13, 15, 17, and 19 TeV for constructive interference, and pure DY production (corresponding to infinite Λ). For each case, three separate samples were generated, corresponding to minimum $\sqrt{\hat{s}}$ values of (300, 500, 800) GeV, with approximately (50k, 25k, and 25k) events per sample, respectively. The $\sqrt{\hat{s}}$ values were chosen to provide good coverage over the dilepton mass range of interest. To reduce computation time and sample size, generator-level kinematic filters were applied with $p_T > 40$ GeV and $|\eta| < 2.6$ for muons, and $p_T > 30$ GeV and $|\eta| < 3.0$ for electrons.

The CI/DY signal yields, which are based on the LO PYTHIA event generator, are increased by

a QCD higher order correction factor of 1.3. This mass-independent value is consistent with QCD calculations through Next-to-Next-Leading Order for the Drell–Yan process [37]. After multiplication by 1.3, the pure DY yields were found to be consistent with those from POWHEG over the range of minimum dilepton mass considered in this analysis.

There are two studies that address NLO QED corrections to the POWHEG DY yields. One is a study [29] based on the HORACE [38–43] 3.1 event generator. Results from this study show, in the dimuon channel, a slightly negative correction which increases in magnitude with dimuon mass. For $M_{\mu\mu}^{\text{min}} = 1500\,\text{GeV}$, i.e., for the cumulative yield of all dimuon masses above 1500 GeV, the factor is 0.94. However, the same HORACE study shows a near cancellation between NLO diagrams and photon induced diagrams for dielectrons, which is contrary to theoretical expectation that the dimuon and dielectron corrections should be similar. The QED k-factor has also been calculated using the FEWZ generator [44] in the dimuon channel and this gave a slightly positive correction, also increasing in magnitude with mass. Given the internal inconsistency in the HORACE study and the disagreement between HORACE and FEWZ for the dimuon channel, we do not apply a QED k-factor to either the dimuon or dielectron DY estimates but assign a 10% yield uncertainty to cover differences between the HORACE and FEWZ results.

4.3 Non-DY backgrounds

While the major source of SM dilepton production is the DY process, a relatively small number of events are due to other SM processes. The simulation samples used to predict the net yield from non-DY sources are summarized in Table 1, with the principal contributions coming from $t\bar{t}$ and diboson production. Wherever possible the non-DY yields determined from the samples have been scaled to account for higher-order QCD diagrams.

In the dielectron channel, another significant source of non-DY dielectrons is the case when one or more jets are mis-identified as electrons. This contribution is estimated by determining, as a function of p_{T} and η, the probability for a jet to be misreconstructed and then applying these probabilities to dijets in data and jets in the W+jets and γ+jets MC samples. The resulting "fake" rate is dominated by dijets where both jets are misreconstructed and is comparable to the $t\bar{t}$ and diboson rates. Based on the difference in fake rate estimated from data using different analysis techniques, a 40% systematic uncertainty is assigned to the final value [29].

4.4 Expected event yields for DY and non-DY production

The event yields expected for the various types of non-DY backgrounds in the dimuon channel are shown in Table 2 along with the DY background for an integrated luminosity of $20\,\text{fb}^{-1}$. The $20\,\text{fb}^{-1}$ value was chosen to facilitate comparison between the dimuon and dielectron channels. The yields are shown for different choices of M^{min}. Some processes are grouped together since the expected yields are small. Non-DY yields are small compared to DY yields for all values of M^{min}, although the non-DY relative uncertainties are much larger than the DY relative uncertainties for M^{min} values above 1000 GeV.

The event yields expected for various types of non-DY backgrounds in the dielectron channel are presented in Table 3 along with the DY yields as a function of M_{ee}^{min} . For dielectrons, as for dimuons, the non-DY contributions are small. Also, the expected yields for the DY process are similar for the dimuon and dielectron channels.

Table 1: Simulation samples used for non-DY background estimation.

Process	Generator	Kinematic cuts $\sqrt{\hat{s}}$, $\hat{p}_T$, and p_T in GeV	# Events (approx.)	σ (pb)
$\tau^+\tau^-$	POWHEG	$\sqrt{\hat{s}} > 20$	3.3M	1.92×10^3
$t\bar{t}$	POWHEG	no cuts	21.6M	2.34×10^2
	POWHEG	$\sqrt{\hat{s}} > 1000$	1.2M	3.28
tW	POWHEG	no cuts	500k	1.11×10^1
$\bar{t}W$	POWHEG	no cuts	500k	1.11×10^1
WW	PYTHIA	no cuts	10M	5.48×10^1
WZ	PYTHIA	no cuts	10M	3.32×10^1
ZZ	PYTHIA	no cuts	10M	17.7
W+jets	MADGRAPH	no cuts	18M	3.63×10^4
QCD μ enriched	PYTHIA	$\hat{p}_T > 20$ $p_T^\mu > 15$ $\lvert\eta(\mu)\rvert < 2.5$	2.1M	1.35×10^5
γ + jets	PYTHIA	$15 < \hat{p}_T < 30$	2M	2.00×10^5
		$30 < \hat{p}_T < 50$		1.99×10^4
		$50 < \hat{p}_T < 80$		3.32×10^3
		$80 < \hat{p}_T < 120$		5.58×10^2
		$120 < \hat{p}_T < 170$		1.08×10^2
		$170 < \hat{p}_T < 300$		3.01×10^1
		$300 < \hat{p}_T < 470$		2.14
		$470 < \hat{p}_T < 800$		2.12×10^{-1}
		$800 < \hat{p}_T < 1400$		7.08×10^{-3}
		$1400 < \hat{p}_T < 1800$		4.51×10^{-5}
		$\hat{p}_T > 1800$		1.87×10^{-6}

5 Systematic uncertainties

Systematic uncertainties in the predicted event yields are summarized in Table 4 for dimuons and Table 5 for dielectrons. These are determined at each value of M^{min}, although only some of the uncertainties vary with dilepton invariant mass. Where there is a mass-dependence in the uncertainties a range of values is given corresponding to the M^{min} range from 1000–1800 GeV. As will be seen in Section 7, it is in this range where lower limits are established on the CI energy scale.

For commonality with other CMS analyses the PDF uncertainties are taken from an analysis in which the PDF4LHC weighting procedure [45] was applied to POWHEG DY Monte Carlo samples. In this study [46], yield variations were obtained separately for CTEQ12 [36], MSTW08 [47], and NNPDF21 [48] PDF sets and the final uncertainties are based on the envelopes of the upward and downward yield variations. The relative PDF uncertainties increase with minimum dilepton mass, ranging from about 5% at $M^{\text{min}} = 400$ GeV to 17% at 1800 GeV.

For dimuons there are three separate sources of uncertainty related to alignment [30]: an uncertainty in the p_T scale based on a cosmic ray endpoint study; a 5% uncertainty stemming from differences in muon chamber alignment scenarios; a 3% smearing in muon p_T to account for a possible misalignment in the inner tracker (resolution). As the cosmic ray study probes the existence of "weak modes", which by construction do not exist in the muon alignment scenarios, the three sources of uncertainty are assumed to be uncorrelated. Both the scale and resolution uncertainties increase with $M_{\mu\mu}^{\text{min}}$ and the values shown in Table 4 for $M_{\mu\mu}^{\text{min}} = 1500$ GeV are taken from parameterizations of DY yields given in Ref. [30]. In addition to the scale, resolution, and alignment uncertainties, there is also a mass-independent Z-peak normalization

Table 2: Non-DY and DY event yields predicted in the dimuon channel for 20 fb^{-1}. The diboson category includes WW, WZ, and ZZ events. "Other" includes W+jets, $\bar{t}$W, tW, QCD, and $\tau^+\tau^-$.

$M_{\mu\mu}^{\text{min}}$ (GeV)	$t\bar{t}$	Diboson	Other	DY
400	194.0	85.9	27	1430
500	59.4	37.9	8.1	599
600	19.4	17.6	4.5	271
700	7.9	9.5	1.4	148
800	3.5	5.4	1.4	80.3
900	1.8	3.0	0.9	46.0
1000	0.4	1.6	0.0	26.9
1100	0.7	0.9	0.0	16.3
1200	0.4	0.7	0.0	10.1
1300	0.2	0.4	0.0	6.23
1400	0.2	0.3	0.0	3.99
1500	0.1	0.0	0.0	2.58
1600	0.0	0.0	0.0	1.70
1700	0.0	0.0	0.0	1.13
1800	0.0	0.0	0.0	0.76

Table 3: Non-DY and DY event yields predicted in the dielectron channel for 20 fb^{-1}. The jets category includes W+jets and γ+jets. "Other" includes $\bar{t}$W, tW, and $\tau^+\tau^-$.

M_{ee}^{min} (GeV)	$t\bar{t}$	Jets	Diboson	Other	DY
400	139.0	73.8	76.0	15.7	1191
500	41.2	30.4	28.8	5.4	517
600	15.8	12.9	11.6	1.3	246
700	3.9	5.7	5.2	0.9	126
800	1.3	2.8	2.8	0.9	68.1
900	0.6	1.2	2.0	0.9	39.2
1000	0.2	0.6	1.4	0.4	23.1
1100	0.4	0.3	0.7	0.4	13.8
1200	0.0	0.2	0.4	0.0	8.55
1300	0.0	0.1	0.3	0.0	5.39
1400	0.0	0.1	0.2	0.0	3.45
1500	0.0	0.0	0.1	0.0	2.22
1600	0.0	0.0	0.0	0.0	1.43
1700	0.0	0.0	0.0	0.0	0.94
1800	0.0	0.0	0.0	0.0	0.61

uncertainty of 3% [29] based on variations in the dimuon reconstruction efficiency from the Z-peak mass to 3 TeV. Finally, there are 3–5% variations in yield for $M_{\mu\mu}^{\text{min}}$ values above 1000 GeV stemming from the statistical uncertainties in the non-DY MC samples.

For dielectrons the largest source of uncertainty is due to PDF variations as determined from the previously described PDF envelope. This is followed by a mass-dependent yield uncertainty that follows from a 1% uncertainty in the in the electron energy scale [29]. Next in magnitude is a 5% uncertainty in yield due to electron reconstruction efficiency [29]. As in the case of the dimuons, there are 3–5% variations due to uncertainties in the non-DY background, which include both the MC sample statistics and an assumbed 40% systematic uncertainty in the "fake" rate.

There is an assumed 3% uncertainty for higher order QCD corrections in DY production for both dimuons and dielectrons. Similarly, the uncertainty related to QED higher order diagrams, which is taken as the size of the mass-dependent correction determined for dimuons, is applied

Table 4: Systematic uncertainties on dimuon yields. Where the uncertainties are mass dependent, they are quoted for the $M_{\mu\mu}^{\min}$ range 1000–1800 GeV.

Source	Rel. Uncert. (%)
Momentum scale	16–37
PDF	10–17
QED higher order corrections	10
Momentum resolution	3–6
Muon alignment	5
Non-DY MC statistics	3–5
Muon reconstruction	3
QCD higher order corrections	3

Table 5: Systematic uncertainties on dielectron yields. Where the uncertainties are mass dependent, they are quoted for the $M_{ee}^{\min}$ range 1000–1800 GeV.

Source	Rel. Uncert. (%)
PDF	10–17
QED higher order corrections	10
Electron energy scale	5–8
Electron reconstruction	5
Non-DY MC statistics and fake rate	3–5
QCD higher order corrections	3

to both dimuons and dielectrons.

The measured integrated luminosity is used to normalize the non-DY backgrounds. The uncertainty in the luminosity, 2.6% [49], does not make a significant contribution to the uncertainty in non-DY backgrounds.

All other sources of uncertainty, for example the statistical uncertainty in the DY samples or the uncertainty in the non-DY yields given the luminosity uncertainty, are negligible and are not considered.

The total relative uncertainty in the predicted number of events for SM dilepton production, including statistical and systematic contributions, is shown in Fig. 2 for dimuons and dielectrons as a function of $M^{\min}$ in GeV units. The $\mu\mu$(ee) uncertainty increases from 15%(14%) for $M^{\min}$ = 400 GeV to 43%(23%) for at $M^{\min} = 1800$ GeV.

6 Dilepton invariant mass spectra

The measured dimuon mass distribution is shown in Figs. 3a (differential) and 3b (integral), and similarly, the reconstructed dielectron distribution is given in Figs. 4a and 4b. The integral plots show the number of events with invariant mass greater than $M^{\min}$. Error bars for the data points reflect statistical (Poisson) uncertainties. All of the plots begin at 300 GeV, which is well below the region of maximum sensitivity to CI signals (for Λ values that have not already been ruled out). The largest dimuon and dielectron masses observed in data are 1.82 TeV and 1.78 TeV, respectively. Included with the data distributions are representative predictions for CI/DY production with Λ values of 11, 13, and 15 TeV. Non-DY SM backgrounds are included.

The data/prediction comparison figures also show the ratio of observed to predicted events in the SM for the differential spectrum. Error bars include uncertainties from the data and pre-

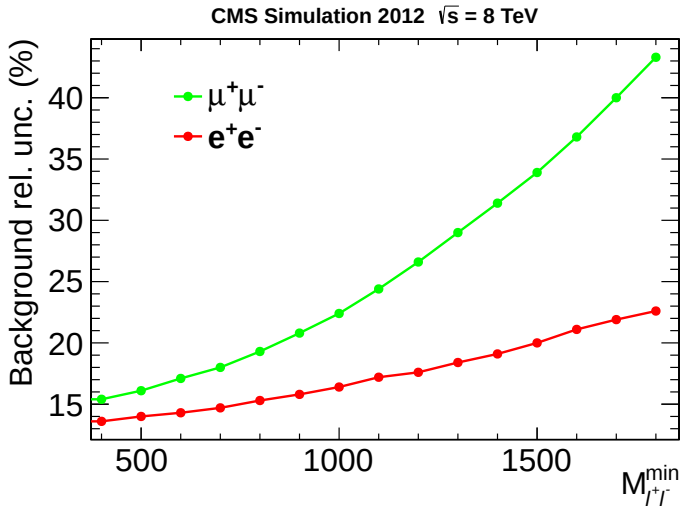

Figure 2: Total relative uncertainty in the SM predicted yield as a function of $M^{\min}$.

diction. The ratios for both dimuon and dielectron spectra are consistent with unity, indicating that the data are consistent with the SM.

7 Lower limits on Λ

Since the data are consistent with the SM, we set lower limits on Λ in the context of the LLIM. The expected and observed 95% CL lower limits on Λ are determined in a Bayesian approach where a flat cross section is assumed as a prior. Limits are determined for $M^{\min}$ values starting with 400 GeV and going up to 1800 GeV in steps of 100 GeV.

The limit setting procedure determines a 95% CL interval for a possible signal taking into account fluctuations of the expected SM background. Since the DY background yield is normalized to the Z-peak, the DY prediction is independent of the luminosity measurement and the 2.6% luminosity uncertainty is not included in the limit calculation. The signal acceptance uncertainties, described in Ref. [29], and the SM background yield uncertainties are treated as nuisance parameters with lognormal distributions.

Dimuon event yields for data and yields predicted by the SM and the LLIM (plus non-DY backgrounds) are shown in Table 6 for destructive interference and Table 7 for constructive interference. For the SM yield prediction the uncertainty is also given. Similarly, Tables 8 and 9 show the dielectron event yields.

For dimuons, the observed and expected lower limits on Λ at 95% CL as a function of $M^{\min}_{\mu\mu}$ for destructive and constructive interference are shown in Figs. 5a and 5b. The value of $M^{\min}_{\mu\mu}$ where the expected limit peaks is 1500 GeV for destructive interference and 1200 GeV for constructive interference. For these values of $M^{\min}_{\mu\mu}$, the observed (expected) limit on Λ is 12.0 TeV (13.0 TeV) for destructive interference and 15.2 TeV (16.9 TeV) for constructive interference. The observed limits lie mainly within the 1σ expected band with an excursion into the 2σ band where observed number of events has an upward fluctuation. For the dielectron channel, shown in Figs. 6a and 6b, the expected limit versus $M^{\min}_{ee}$ is similar to the dimuon channel. The expected dielectron limit peaks at $M^{\min}_{ee} = 1300$ and 1100 GeV for destructive and constructive interference, respectively. For these values of $M^{\min}_{ee}$, the observed (expected) limits are 13.5 TeV

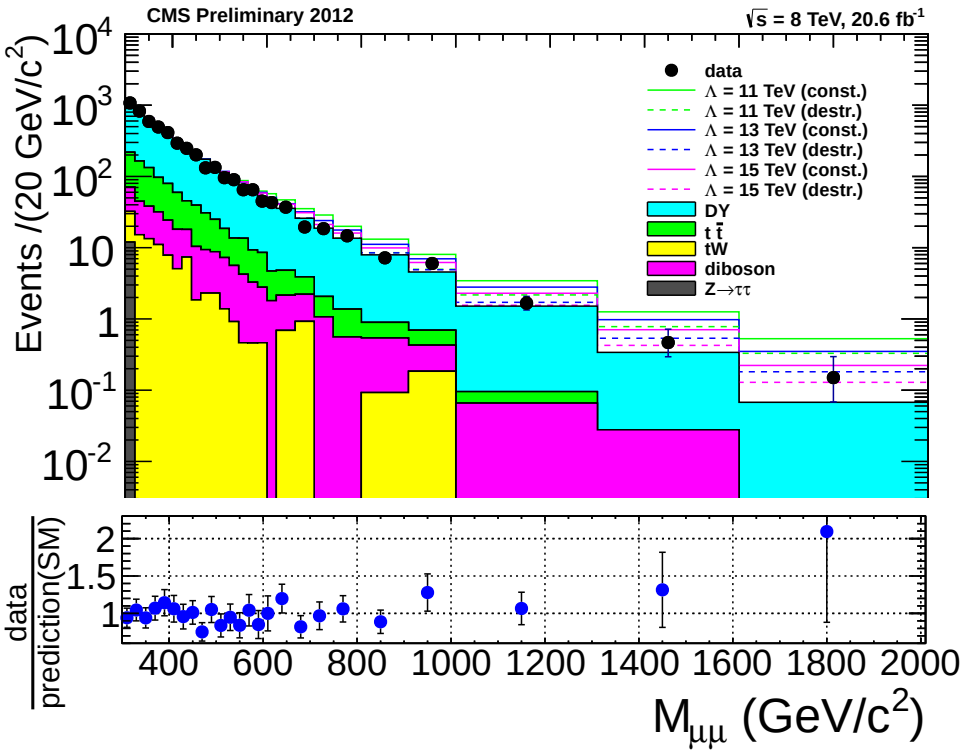

(a)

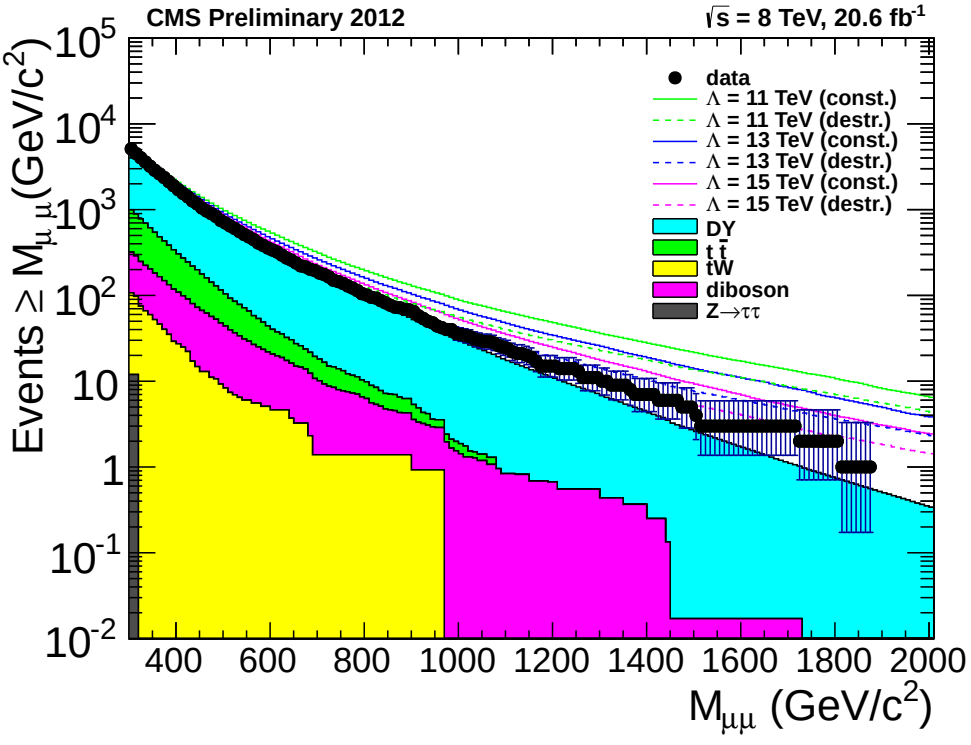

(b)

Figure 3: The dimuon mass spectrum for 20.6 fb^{-1} shown with predictions for the SM and the LLIM with destructive and constructive interference. The differential spectrum in M is shown in (a) with variable bin width. The integral spectrum is shown in (b). Error bars for data points show statistical (Poisson) uncertainties. In the plot below (a), the error bars include statistical uncertainties in the data and both statistical and systematic uncertainties in the prediction.

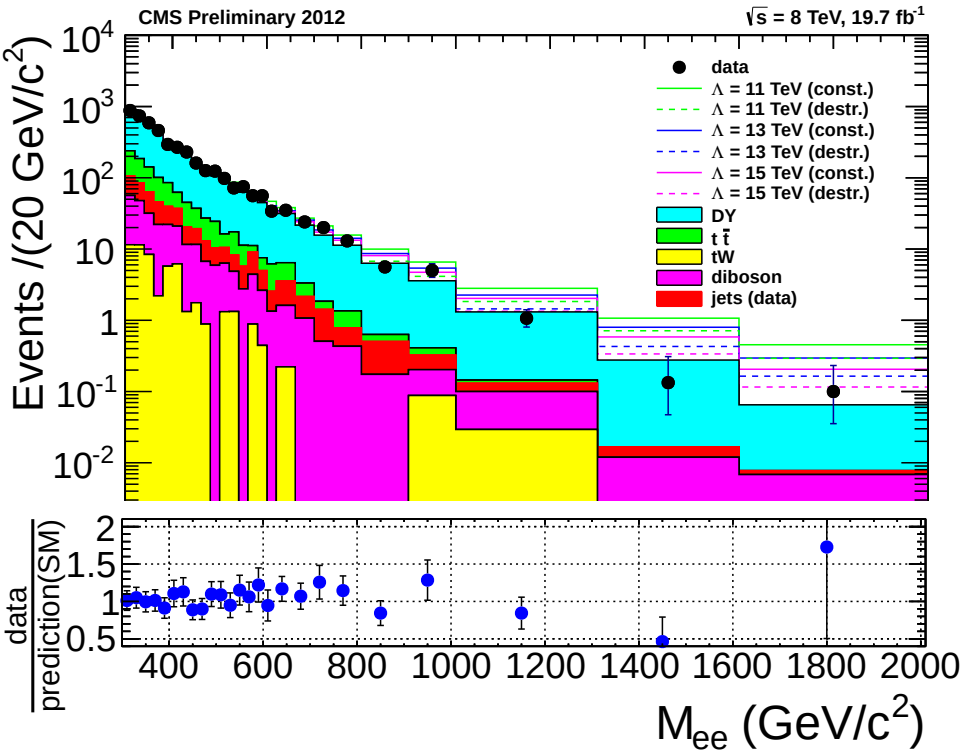

(a)

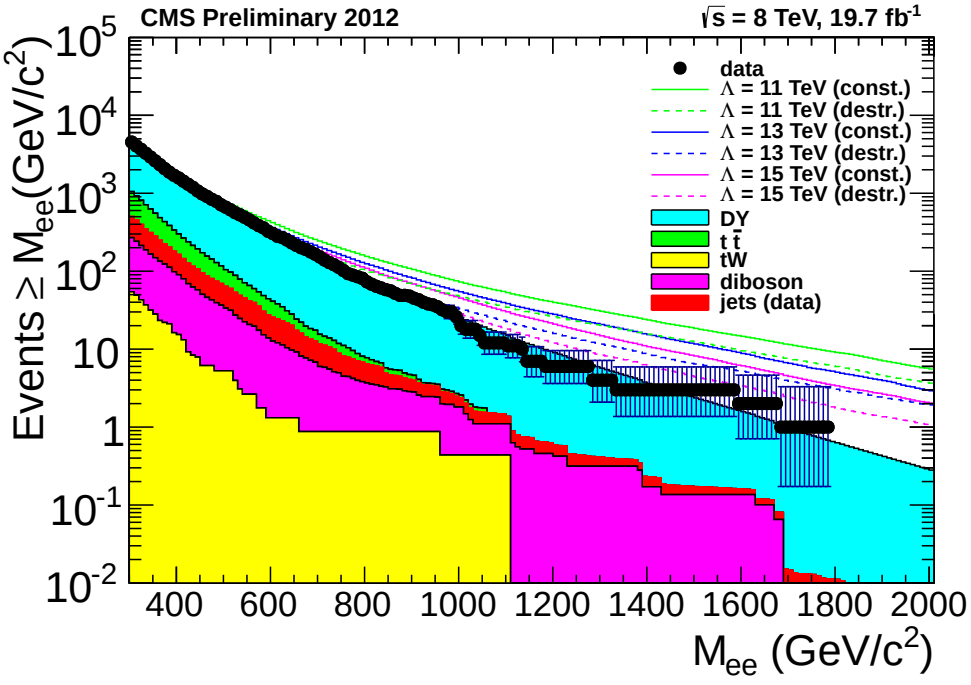

(b)

Figure 4: The dielectron mass spectrum for 19.7 fb^{-1} shown with predictions for the SM and the LLIM with destructive and constructive interference. The differential spectrum in M is shown in (a) with variable bin width. The integral spectrum is shown in (b). Error bars for data points show statistical (Poisson) uncertainties. In the plot below (a), the error bars include statistical uncertainties in the data and both statistical and systematic uncertainties in the prediction.

Table 6: Observed and predicted number of dimuon events corresponding to an integrated luminosity of 20.6 fb^{-1}. The CI/DY predictions are shown for destructive interference based on the LLIM. Both the SM and CI/DY predictions include small contributions from non-DY backgrounds. The missing CI/DY entries correspond to values that are less than the $\Lambda = \infty$ prediction. In the region where we set limits, the destructive CI/DY values always exceed the SM prediction.

$M_{\mu\mu}^{\min}$ (GeV)	500	600	700	800	900	1000	1100	1200	1300	1400	1500
Source	Number of Events										
data	699	338	182	101	65	35	24	15	10	7	4
SM pred.	721.2	320.2	171.1	92.7	52.9	29.7	18.3	11.4	7.1	4.6	2.8
σ(SM pred.)	116.3	54.6	30.8	17.9	11.0	6.7	4.5	3.0	2.1	1.4	0.9
Λ (TeV)											
20											3.0
19								12.0	7.8	5.1	3.2
18							19.2	12.4	8.1	5.4	3.4
17						31.2	19.8	13.0	8.6	5.8	3.8
16						32.3	20.8	13.9	9.4	6.4	4.3
15					56.6	34.0	22.3	15.1	10.5	7.4	5.1
14				100	59.4	36.6	24.5	17.1	12.1	8.7	6.2
13			180	105	63.8	40.6	27.9	19.9	14.5	10.7	7.9
12			189	113	70.9	46.7	33.1	24.4	18.3	13.9	10.6
11	758	365	203	126	82.3	56.7	41.5	31.5	24.3	18.9	14.7
10	787	393	228	148	101	73.1	55.4	43.1	34.1	27.0	21.6

Table 7: Observed and predicted number of dimuon events corresponding to an integrated luminosity of 20.6 fb^{-1}. The CI/DY (Λ) yields are shown for constructive interference based on the LLIM.

$M_{\mu\mu}^{\min}$ (GeV)	500	600	700	800	900	1000	1100	1200	1300	1400	1500
Source	Number of Events										
data	699	338	182	101	65	35	24	15	10	7	4
SM pred.	721.2	320.2	171.1	92.7	52.9	29.7	18.3	11.4	7.1	4.6	2.8
σ(SM pred.)	116.3	54.6	30.8	17.9	11.0	6.7	4.5	3.0	2.1	1.4	0.9
Λ (TeV)											
20	792	381	202	115	68.3	41.0	26.9	17.9	12.2	8.5	5.8
19	798	386	205	118	70.2	42.5	28.0	18.9	13.0	9.1	6.3
18	805	392	210	121	72.6	44.3	29.5	20.0	13.9	9.8	6.9
17	814	399	215	124	75.6	46.6	31.3	21.5	15.0	10.7	7.6
16	824	408	222	129	79.4	49.6	33.8	23.4	16.6	12.0	8.6
15	838	420	230	136	84.5	53.6	37.0	26.0	18.6	13.6	9.9
14	856	435	242	145	91.4	59.0	41.3	29.5	21.4	15.8	11.7
13	881	454	257	157	101	66.6	47.4	34.3	25.3	18.9	14.2
12	915	482	278	173	114	77.4	56.1	41.3	30.9	23.4	17.8
11	964	520	308	198	134	93.5	69.0	51.5	39.2	30.2	23.2
10	1036	577	354	236	165	118.2	88.9	67.4	52.0	40.6	31.6

Table 8: Observed and predicted number of dielectron events corresponding to an integrated luminosity of 19.7 fb^{-1}. The CI/DY predictions are shown for destructive interference based on the LLIM. Both the SM and CI/DY predictions include small contributions from non-DY backgrounds. The missing CI/DY entries correspond to values that are less than the $\Lambda = \infty$ prediction. In the region where we set limits, the destructive CI/DY values always exceed the SM prediction.

$M_{ee}^{\min}$ (GeV)	500	600	700	800	900	1000	1100	1200	1300	1400	1500
Source	Number of Events										
data	661	304	152	73	45	20	11	6	4	3	3
SM pred.	623.9	288.5	142.5	76.1	44.0	25.8	15.3	9.2	5.8	3.7	2.4
σ(SM pred.)	87.5	41.3	21.0	11.6	6.9	4.2	2.6	1.6	1.1	0.7	0.5
Λ (TeV)											
20									6.0	3.9	2.5
19								9.6	6.2	4.1	2.7
18								9.9	6.5	4.3	2.9
17							16.4	10.4	6.9	4.7	3.2
16						27.4	17.2	11.1	7.6	5.3	3.7
15						28.7	18.4	12.2	8.5	6.0	4.3
14					47.3	30.7	20.2	13.7	9.8	7.1	5.2
13				80.3	50.7	33.8	22.9	16.1	11.8	8.8	6.6
12				86.5	56.2	38.6	27.1	19.7	14.9	11.4	8.8
11			156	97.1	65.2	46.4	33.8	25.4	19.7	15.4	12.1
10	616	313	178	115	80.4	59.4	44.8	34.8	27.7	21.8	17.5

Table 9: Observed and predicted number of dielectron events corresponding to an integrated luminosity of 19.7 fb^{-1}. The CI/DY (Λ) yields are shown for constructive interference based on the LLIM.

$M_{ee}^{\min}$ (GeV)	500	600	700	800	900	1000	1100	1200	1300	1400	1500
Source	Number of Events										
data	661	304	152	73	45	20	11	6	4	3	3
SM pred.	623.9	288.5	142.5	76.1	44.0	25.8	15.3	9.2	5.8	3.7	2.4
σ(SM pred.)	87.5	41.3	21.0	11.6	6.9	4.2	2.6	1.6	1.1	0.7	0.5
Λ (TeV)											
20	635	312	162	91.6	55.0	34.1	21.6	14.1	9.6	6.6	4.7
19	640	316	165	93.5	56.5	35.2	22.5	14.8	10.2	7.1	5.1
18	646	320	168	95.8	58.3	36.6	23.6	15.7	10.9	7.7	5.6
17	653	325	172	98.8	60.6	38.3	25.1	16.9	11.9	8.4	6.2
16	661	331	177	103	63.7	40.6	27.0	18.4	13.1	9.4	7.0
15	672	339	183	108	67.7	43.7	29.5	20.5	14.8	10.8	8.1
14	686	350	191	114	73.1	47.9	33.0	23.3	17.0	12.6	9.5
13	705	365	203	124	80.5	53.9	37.9	27.2	20.2	15.1	11.6
12	731	385	219	137	91.2	62.5	44.9	32.8	24.7	18.8	14.6
11	766	414	242	156	107	75.3	55.4	41.3	31.5	24.3	19.0
10	818	458	278	186	131	95.2	71.7	54.3	42.0	32.8	25.8

(12.7 TeV) for destructive interference and 18.3 TeV (16.5 TeV) for constructive interference. The observed limits lie almost entirely in the 1σ expected band.

Under the assumption that the contact interaction with quarks is independent of lepton flavor, the dimuon and dielectron channels can be combined by summing the observed (predicted) yields in the two channels. Uncertainties are added in quadrature, taking into account highly correlated sources such as the PDF variations. The limit results are shown in Figs. 7a and 7b, for destructive and constructive interference, respectively. The observed limits are entirely confined to the 1σ expected band. The observed limits are 13.1 TeV and 16.9 TeV for destructive and constructive interference.

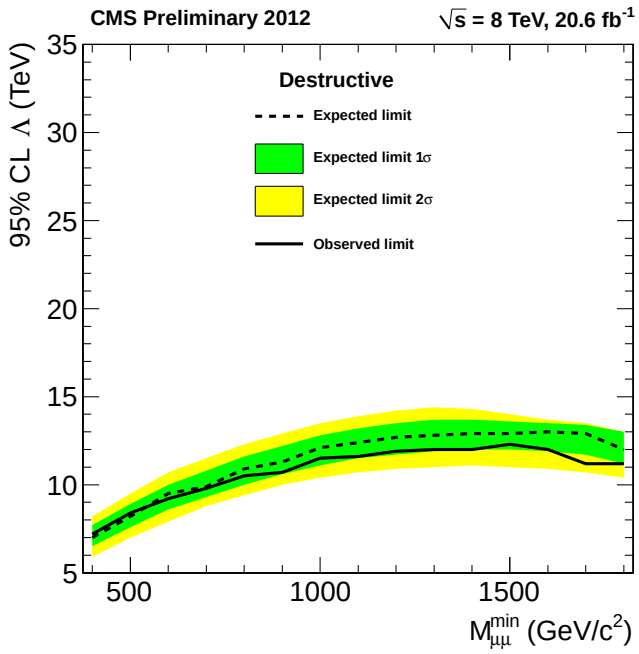

(a)

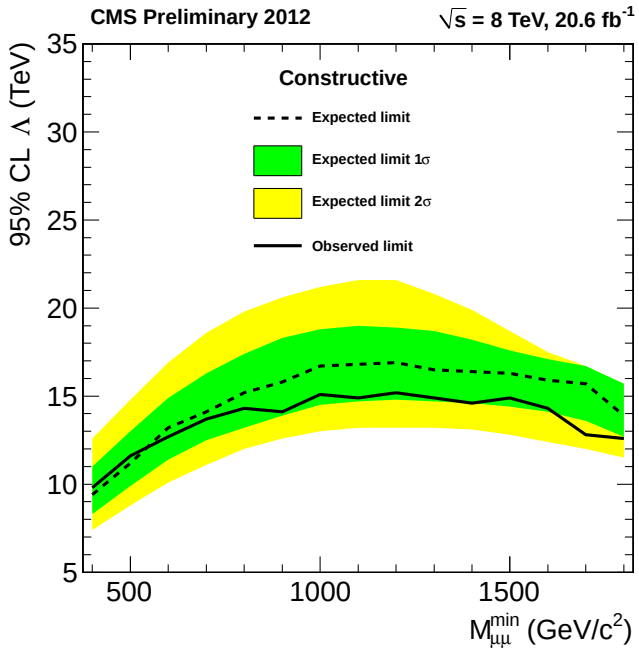

(b)

Figure 5: Observed and expected limits on Λ (dimuon channel) as a function of $M_{\mu\mu}^{\min}$ for (a) destructive interference and (b) constructive interference.

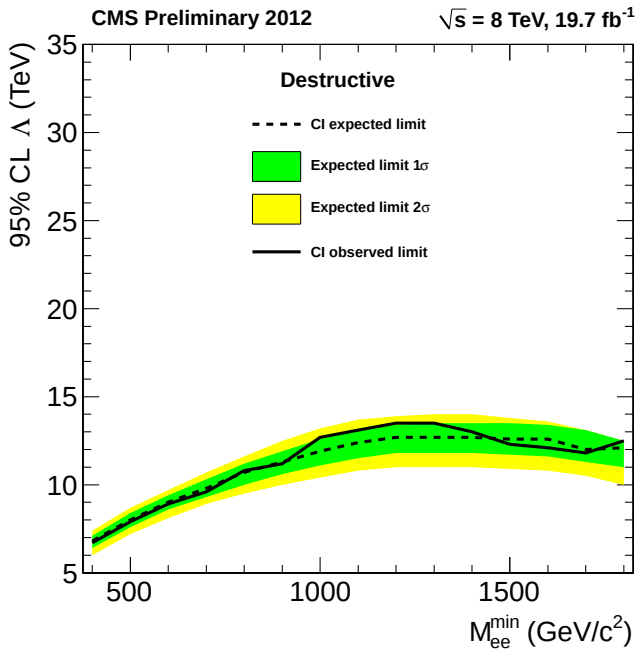

(a)

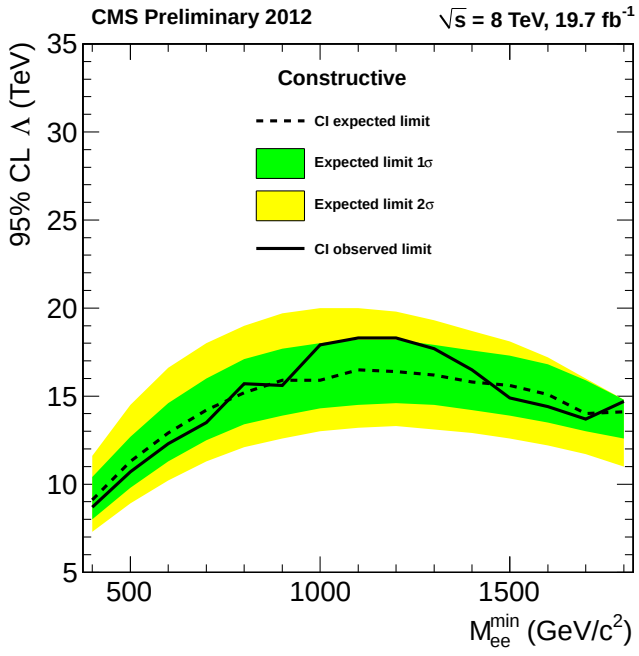

(b)

Figure 6: Observed and expected limits on Λ (dielectron channel) as a function of $M_{ee}^{\min}$ for (a) destructive interference and (b) constructive interference.

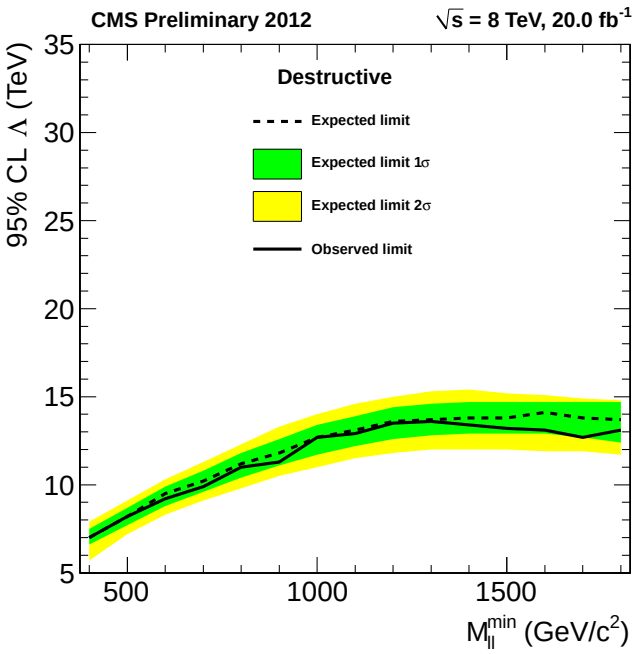

(a)

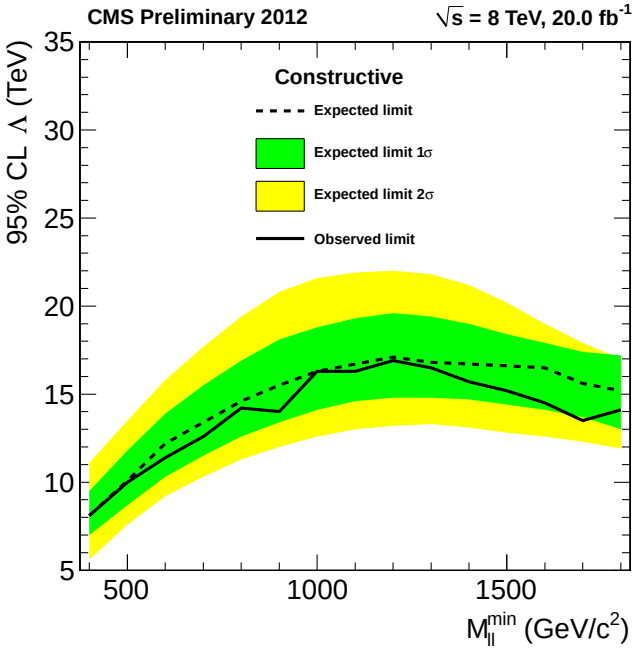

(b)

Figure 7: Observed and expected limits for the combined dimuon and dielectron channels as a function of $M_{ll}^{\min}$ for (a) destructive interference and (b) constructive interference.

8 Summary

Using the CMS detector, the invariant mass distribution of $\mu^+\mu^-$ and e^+e^- pairs produced in pp collisions at a center-of-mass energy of 8 TeV has been measured for integrated luminosities of 20.6 and 19.7 fb^{-1}, respectively. The mass spectra for $M_{ll}^{\text{min}} > 300\,\text{GeV}$ are consistent with Drell–Yan plus other standard model sources of dileptons. Within the context of the left-left isoscalar contact interaction model lower limits at 95% CL are set on the energy scale parameter Λ. For dimuons the limits are 12.4 TeV for destructive interference and 14.8 TeV for constructive interference. Similarly, the dielectron limits are 13.4 TeV for destructive interference and 19.0 TeV for constructive interference. These limits represent significant improvements on the current published values.

References

[1] E. Eichten, K. Lane, and M. Peskin, "New Tests for Quark and Lepton Substructure", *Phys. Rev. Lett.* **50** (1983) 811, doi:10.1103/PhysRevLett.50.811.

[2] E. Eichten et al., "Supercollider Physics", *Rev. Modern Phys.* **56** (1984) 579, doi:10.1103/RevModPhys.56.579.

[3] S. Drell and T. Yan, "Massive Lepton-Pair Production in Hadron-Hadron Collisions at High Energy", *Phys. Rev. Lett.* **25** (1970) 316, doi:10.1103/PhysRevLett.25.316.

[4] T. Sjöstrand, S. Mrenna, and P. Skand, "Pythia 6.4 Physics and Manual", *JHEP* **05** (2006) 026, doi:10.1088/1126-6708/2006/05/026.

[5] ALEPH Collaboration, "Fermion pair production in e^+e^- collisions at 189–209 GeV and constraints on physics beyond the standard model", *Eur. Phys. J. C* **49** (2007) 411, doi:10.1140/epjc/s10052-006-0156-8.

[6] DELPHI Collaboration, "Measurement and interpretation of fermion-pair production at LEP energies above the Z resonance", *Eur. Phys. J. C* **45** (2006) 589, doi:10.1140/epjc/s2005-02461-0.

[7] L3 Collaboration, "Search for manifestations of new physics in fermion-pair production at LEP", *Phys. Lett. B* **489** (2000) 81, doi:10.1016/S0370-2693(00)00887-X.

[8] OPAL Collaboration, "Production of fermion-pair events in e^+e^- collisions at 161 GeV centre-of-mass energy", *Phys. Lett. B* **391** (1997) 221, doi:10.1016/S0370-2693(97)81627-9.

[9] OPAL Collaboration, "Tests of the standard model and constraints on new physics from measurements of fermion-pair production at 189–209 GeV at LEP", *Eur. Phys. J. C* **33** (2004) 173, doi:10.1140/epjc/s2004-01595-9.

[10] H1 Collaboration, "Search for Contact Interactions in $e^{\pm}p$ Collisions at HERA", *Phys. Lett. B* **705** (2011) 52, doi:10.1016/j.physletb.2011.09.109.

[11] ZEUS Collaboration, "Search for contact interactions, large extra dimensions and finite quark radius in ep collisions at HERA", *Phys. Lett. B* **591** (2004) 23, doi:10.1016/j.physletb.2004.03.081.

[12] CDF Collaboration, "Search for New Gauge Bosons in $\bar{p}p$ Collisions at $\sqrt{s} = 1.8$ TeV", *Phys. Rev. Lett.* **68** (1992) 1463, doi:10.1103/PhysRevLett.68.1463.

[13] CDF Collaboration, "Limits on Quark-Lepton Compositeness Scales from Dileptons Produced in 1.8 TeV $p\bar{p}$ Collisions", *Phys. Rev. Lett.* **79** (1997) 2198, doi:10.1103/PhysRevLett.79.2198.

[14] CDF Collaboration, "Search for Quark-Lepton Compositeness and a Heavy W Boson Using the $e\nu$ Channel in $p\bar{p}$ Collisions at $\sqrt{s} = 1.8$ TeV", *Phys. Rev. Lett.* **87** (2001) 231803, doi:10.1103/PhysRevLett.87.231803.

[15] CDF Collaboration, "Search for $Z' \to e^+e^-$ Using Dielectron Mass Angular Distribution", *Phys. Rev. Lett.* **96** (2006) 211801, doi:10.1103/PhysRevLett.96.211801.

[16] D0 Collaboration, "Measurement of the High-Mass Drell-Yan Cross Section and Limits on Quark-Electron Compositeness Scales", *Phys. Rev. Lett.* **82** (1999) 4769, doi:10.1103/PhysRevLett.82.4769.

[17] D0 Collaboration, "Measurement of Dijet Angular Distribution at $\sqrt{s} = 1.96$ TeV and Searches for Quark Compositeness and Extra Spatial Dimensions", *Phys. Rev. Lett.* **103** (2009) 191803, doi:10.1103/PhysRevLett.103.191803.

[18] ATLAS Collaboration, "Search for quark contact interactions in dijet angular distributions in pp collisions at $\sqrt{s} = 7$ TeV measured with the ATLAS detector", *Phys. Lett. B* **694** (2011) 327, doi:10.1016/j.physletb.2010.10.021.

[19] ATLAS Collaboration, "Search for contact interactions in dimuon events from pp collision at $\sqrt{s} = 7$ TeV with the ATLAS detector", *Phys. Rev. D* **84** (2011) 011101, doi:10.1103/PhysRevD.84.011101.

[20] ATLAS Collaboration, "Search for contact interactions in dimuon events from pp collisions at $\sqrt{s} = 7$ TeV with the ATLAS Detector", *Phys. Lett. B* **712** (2012) 40, doi:10.1016/j.physletb.2012.04.026.

[21] ATLAS Collaboration, "Search for contact interactions and large extra dimensions in dilepton events from pp collisions at $\sqrt{s} = 7$ TeV with the ATLAS detector", *Phys. Rev. D* **87** (2013) 015010, doi:10.1103/PhysRevD.87.015010, arXiv:1211.1150.

[22] CMS Collaboration, "Search for Quark Compositeness with the Dijet Centrality Ratio in pp Collisions at $\sqrt{s} = 7$ TeV", *Phys. Rev. Lett.* **105** (2010) 262001, doi:10.1103/PhysRevLett.105.262001.

[23] CMS Collaboration, "Search for quark compositeness in dijet angular distributions from pp collisions at $\sqrt{s} = 7$ TeV", *JHEP* **1205** (2012) 055, doi:10.1007/JHEP05(2012)055.

[24] CMS Collaboration, "Updated Search for New Physics in Highly Boosted Z^0 Decays to Dimuon in pp Collisions at $\sqrt{s} = 7$ TeV", CMS Physics Analysis Summary CMS-PAS-EXO-11-025, 2012.

[25] CMS Collaboration, "Search for contact interactions using the inclusive jet p_T spectrum in pp collisions at $\sqrt{s} = 7$ TeV", *Phys. Rev. D* **87** (2013) 052017, doi:10.1103/PhysRevD.87.052017, arXiv:1301.5023.

[26] CMS Collaboration, "Search for contact interactions in opposite-sign dimuon events in pp collisions at $\sqrt{s} = 7$ TeV", *Phys. Rev. D* **87** (2013) 032001, doi:10.1103/PhysRevD.87.032001, arXiv:1212.4563.

[27] K. Cheung, "Constraints on electron-quark contact interactions and implications to models of leptoquarks and extra Z bosons", *Phys. Lett. B* **517** (2001) 167, doi:10.1016/S0370-2693(01)00973-X, arXiv:hep-ph/0106251.

[28] CMS Collaboration, "The CMS experiment at the CERN LHC", *JINST* **03** (2006) S08004, doi:10.1088/1748-0221/3/08/S08004.

[29] CMS Collaboration, "Search for Resonances in the Dilepton Mass Distribution in pp Collisions at sqrt(s) = 8 TeV", CMS Physics Analysis Summary CMS-PAS-EXO-12-061, 2013.

[30] CMS Collaboration, "Search for Extra Dimensions in Dimuon Events in pp Collisions at sqrt(s) = 8 TeV", CMS Physics Analysis Summary CMS-PAS-EXO-12-027, 2013.

[31] CMS Collaboration, "Search for Large Extra Spatial Dimensions in Dielectron Production with the CMS Detector", CMS Physics Analysis Summary CMS-PAS-EXO-12-031, 2013.

[32] M. Cacciari and G. P. Salam, "Pileup subtraction using jet areas", *Phys. Lett. B* **659** (2008) 119, doi:10.1016/j.physletb.2007.09.077, arXiv:0707.1378.

[33] GEANT4 Collaboration, "GEANT4: A simulation toolkit", *Nucl. Instrum. Meth. A* **506** (2003) 250, doi:10.1016/S0168-9002(03)01368-8.

[34] S. Alioli, P. Nason, C. Oleari, and E. Re, "NLO vector-boson production matched with shower in POWHEG", *JHEP* **0807** (2008) 060, doi:10.1088/1126-6708/2008/07/060, arXiv:0805.4802.

[35] H. Lai et al., "New parton distributions for collider physics", *Phys. Rev. D* **82** (2010) 074024, doi:10.1103/PhysRevD.82.074024, arXiv:1007.2241.

[36] P. Nadolsky et al., "Implications of CTEQ global analysis for collider observables", *Phys. Rev. D* **78** (2008) 013004, doi:10.1103/PhysRevD.78.013004, arXiv:0802.0007.

[37] S. Catani et al., "Vector Boson Production at Hadron Colliders: A Fully Exclusive QCD Calculation at Next-to-Next-to-Leading Order", *Phys. Rev. Lett.* **103** (209) 082001, doi:10.1103/PhysRevLett.103.082001.

[38] C. Carloni Calame, G. Montagna, O. Nicrosini, and A. Vicini, "Precision electroweak calculation of the production of a high transverse-momentum lepton pair at hadron colliders", *JHEP* **0710** (2007) 109, doi:10.1088/1126-6708/2007/10/109, arXiv:0710.1722.

[39] TeV4LHC-Top and Electroweak Working Group Collaboration, "Tevatron-for-LHC Report: Top and Electroweak Physics", arXiv:0705.3251.

[40] C. Carloni Calame, G. Montagna, O. Nicrosini, and A. Vicini, "Precision electroweak calculation of the charged current Drell-Yan process", *JHEP* **0612** (2006) 016, doi:10.1088/1126-6708/2006/12/016, arXiv:hep-ph/0609170.

[41] C. Buttar et al., "Les houches physics at TeV colliders 2005, standard model and Higgs working group: Summary report", arXiv:hep-ph/0604120.

[42] C. Carloni Calame, G. Montagna, O. Nicrosini, and M. Treccani, "Multiple photon corrections to the neutral-current Drell-Yan process", *JHEP* **0505** (2005) 019, doi:10.1088/1126-6708/2005/05/019, arXiv:hep-ph/0502218.

[43] C. Carloni Calame, G. Montagna, O. Nicrosini, and M. Treccani, "Higher order QED corrections to W boson mass determination at hadron colliders", *Phys. Rev. D* **69** (2004) 037301, doi:10.1103/PhysRevD.69.037301, arXiv:hep-ph/0303102.

[44] R. Gavin et al., "FEWZ 2.0: A code for hadronic Z production at next-to-next-to-leading order", *Comput. Phys. Commun.* **182** (2011) 2388, doi:10.1016/j.cpc.2011.06.008, arXiv:1011.3540.

[45] M. Botje et al., "The PDF4LHC Working Group Interim Recommendations", (2011). arXiv:1101.0538. Unpublished.

[46] CMS Collaboration, "PDF Uncertainties for Z′ searches at 8 TeV", CMS Analysis Note CMS-AN-2012-348, 2012.

[47] A. Martin, W. Stirling, R. Thorne, and G. Watt, "Parton distributions for the LHC", *Eur. Phys. J. C* **63** (2009) 189, doi:10.1140/epjc/s10052-009-1072-5, arXiv:0901.0002.

[48] NNPDF Collaboration, "Fitting Parton Distribution Data with Multiplicative Normalization Uncertainties", *JHEP* **1005** (2010) 075, doi:10.1007/JHEP05(2010)075, arXiv:0912.2276.

[49] CMS Collaboration, "Absolute Calibration of the Luminosity Measurement at CMS: Winter 2012 Update", CMS Physics Analysis Summary CMS-PAS-SMP-12-008, 2012.